

Characterizing the physical conditions of cold/warm gas in submillimeter bright galaxies at $z > 3$

Ken-ichi Tadaki¹

¹National Astronomical Observatory of Japan, 2-21-1 Osawa,
Mitaka-shi, Tokyo 181-8588
tadaki.ken@nao.ac.jp

Abstract

Recent ALMA observations have revealed CO and [CI] spectral line energy distributions (SLED) including mig–J/high–J CO lines and [CI](1–0)/[CI](2–1) lines in submillimeter bright galaxies at $z > 3$. It is important to understand the physical conditions of cold and warm gas in these starburst galaxies, where the core of giant ellipticals is being formed. Combining ngVLA observations of CO(1–0) and CO(2–1) emission lines with ALMA ones, it is possible to separately characterize the physical properties of cold and warm molecular gas and then measure the gas mass without assuming a CO-to-H₂ conversion factor and local thermodynamical equilibrium excitation. Furthermore, the ngVLA-ALMA synergetic observations will reveal the spatial distributions of cold and warm gas, separately.

Key words: galaxies: high-redshift — galaxies: starburst — galaxies: ISM

1. Introduction

Recent deep observations have spectroscopically identified submillimeter bright galaxies (SMGs) at $z = 3 – 6$ (Riechers et al. 2013; Vieira et al. 2013; Yun et al. 2015; Casey et al. 2017; Casey et al. 2019). They are intensively forming stars at more than 1000 times higher rate than the Milky Way and have large gas reservoirs to fuel star formation. They are also the most massive galaxies with a stellar mass of $\log(M_*/M_\odot) \sim 11$ in the early Universe (Michałowski et al. 2014). A large fraction of stars is formed in the central 1 kpc region (Simpson et al. 2015; Ikarashi et al. 2015; Hodge et al. 2016), that is comparable in size to massive, quiescent galaxies at the peak of cosmic star formation history (van Dokkum et al. 2015) and a core of giant elliptical galaxies in the present-day Universe. The compact core must play a primary role in the bulge formation in the most massive galaxies in the early Universe while the physical properties inside the compact starburst region are poorly understood. It is important to understand how SMGs build up a compact core through studies of the physical properties of molecular gas.

COSMOS-AzTEC-1 is a well studied SMG with a wide array of ancillary data, and can serve as a template for starbursts at high-redshift. This is an unlensed SMG at $z_{\text{spec}} = 4.342$ (Yun et al. 2015) and intrinsically has a large stellar mass of $M_* = 9.9^{+0.4}_{-2.6} \times 10^{10} M_\odot$ (Tadaki et al. 2018). Five emission lines (CO(4–3), CO(7–6), CO(12–11), [CI](1–0) and [CI](2–1)) have been detected by ALMA observations (Tadaki et al. 2018; Tadaki et al. 2019). High–J CO lines can be used for tracing warm gas while [CI] lines can be used for tracing cold gas (Weiβ et al. 2005; Brisbin et al. 2019; Valentino et al. 2020). The observed CO and [CI] SLED can not be explained by single component models, indicating that COSMOS-AzTEC-1 has at least two gas components (cold and warm gas). We also find that a high carbon abundance of

$[\text{CI}]/\text{H}_2 > 1 \times 10^{-4}$ is required to reproduce the CO and [CI] SLED even with two component models (Figure 1). The typical value in normal star-forming galaxies is $[\text{CI}]/\text{H}_2 = 3 \times 10^{-5}$ (Papadopoulos & Greve 2004; Weiβ et al. 2003; Weiβ et al. 2005) and the value in the central region of the local starburst galaxy M82 is $[\text{CI}]/\text{H}_2 = 5 \times 10^{-5}$. Such an elevated carbon abundance has been pointed out in Bothwell et al. 2017.

2. Spatially-unresolved observations of CO(1–0) and CO(2–1) line emission

A problem is that the uncertainty on carbon abundance significantly affects the estimate of the gas column density and gas mass. In the case of COSMOS-AzTEC-1 (Figure 1), the estimated gas column density is $N_{\text{CO}} = 8 \times 10^{18} \text{ cm}^{-2}$ for $[\text{CI}]/\text{H}_2 = 5 \times 10^{-5}$ (M82-like) and $N_{\text{CO}} = 6 \times 10^{17} \text{ cm}^{-2}$ for $[\text{CI}]/\text{H}_2 = 2 \times 10^{-4}$. Thus, observations of CO(1–0) and CO(2–1) emission allow us to characterize the physical conditions of cold molecular gas as well as to constrain the carbon abundance. We require the sensitivity of $1\sigma=96 \mu\text{Jy beam}^{-1}$ per 50 km s^{−1} at 21 GHz (for CO(1–0)) and $1\sigma=180 \mu\text{Jy beam}^{-1}$ per 20 km s^{−1} at 42 GHz (for CO(2–1)) (Figure 1). Using ngVLA, we can reach these depths with about 20 minutes on source time and make a systematic survey of CO(1–0) and CO(2–1) line emission for a large sample of bright SMGs at $z > 3$. It is in principle possible to calculate the molecular gas mass from only two [CI] lines. However, this approach requires the assumptions that both [CI] lines are optically thin and are in local thermodynamical equilibrium (LTE), which are not verified by observations of high-redshift starburst galaxies. The proposed study of CO and [CI] SLED through non-LTE modeling will enable us to derive the optical depth and the excitation of these lines. Therefore, we will be able to measure the gas mass without assuming a CO-to-H₂ conversion factor and LTE excitation.

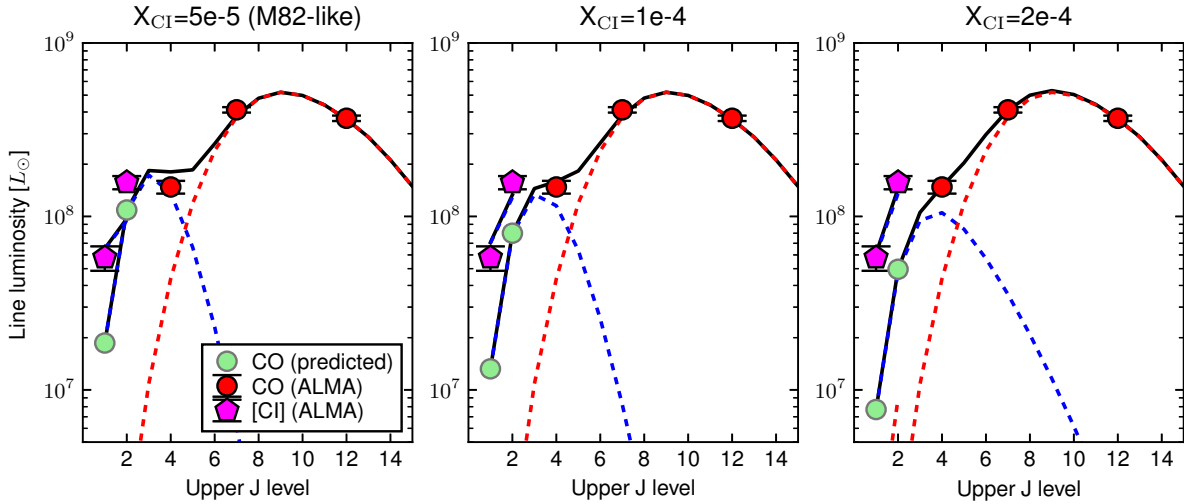


Fig. 1. CO and [C I] SLEDs of COSMOS-AzTEC-1 at $z = 4.3$. Red circles and magenta pentagons show the galaxy-integrated luminosities of CO(4–3), CO(7–6), CO(12–11), [C I](1–0) and [C I](2–1) lines from the ALMA observations (Tadaki et al. 2018; Tadaki et al. 2019). From left to right, we show the best-fit models (blue dashed lines for cold component, red dashed lines for warm one and black solid lines for the total) of the RADEX (van der Tak et al. 2007) non-LTE modeling results in three cases of carbon abundance. Green circles show the predicted luminosities of CO(1–0) and CO(2–1) lines in three cases of [C I] abundance.

3. Spatially-resolved observations of CO(1–0) and CO(2–1) line emission

A next step is to spatially resolve the CO(1–0) and CO(2–1) line emission, tracing cold gas. Hodge et al. 2012 have revealed the spatial distribution of CO(2–1) line emission in GN20, a bright SMG at $z = 4.2$ (Hodge et al. 2012), and this is the only success so far. As the difficulty mainly comes from a low luminosity and an extended structure, it is challenging to spatially resolve the low- J CO emission at 1 kpc-($0''.1$ – $0''.2$) resolution with the current JVLA sensitivity. Figure 2 shows the results from simulations of ngVLA observations with 8 hours integration. The input model has the same CO excitation as in GN20 (Carilli et al. 2010; Carilli et al. 2011) and an exponential disk with $0''.4$ (2.7 kpc), which is a factor of 2–3 larger than in the CO(4–3) and CO(7–6) emission. The ngVLA-ALMA synergistic observations will enable us to constrain the spatially-resolved CO SLEDs to separately map the distributions of cold and warm gas component as well as to characterize the gas density and the gas kinetic temperature of each component.

References

- Bothwell, M. S., Aguirre, J. E., Aravena, M., et al. 2017, MNRAS, 466, 2825
 Brisbin, D., Aravena, M., Daddi, E., et al. 2019, A&A, 628, A104
 Carilli, C. L., Hodge, J., Walter, F., et al. 2011, ApJL, 739, L33
 Carilli, C. L., Daddi, E., Riechers, D., et al. 2010, ApJ, 714, 1407
 Casey, C. M., Cooray, A., Killi, M., et al. 2017, ApJ, 840, 101
 Casey, C. M., Zavala, J. A., Aravena, M., et al. 2019, ApJ, 887, 55
 Hodge, J. A., Carilli, C. L., Walter, F., et al. 2012, ApJ, 760, 11
 Hodge, J. A., Swinbank, A. M., Simpson, J. M., et al. 2016, ApJ, 833, 103
 Ikarashi, S., Ivison, R. J., Caputi, K. I., et al. 2015, ApJ, 810, 133

- Michałowski, M. J., Hayward, C. C., Dunlop, J. S., et al. 2014, A&A, 571, A75
 Papadopoulos, P. P., & Greve, T. R. 2004, ApJL, 615, L29
 Riechers, D. A., Bradford, C. M., Clements, D. L., et al. 2013, Nature, 496, 329
 Simpson, J. M., Smail, I., Swinbank, A. M., et al. 2015, ApJ, 799, 81
 Tadaki, K., Iono, D., Yun, M. S., et al. 2018, Nature, 560, 613
 Tadaki, K.-i., Iono, D., Hatsukade, B., et al. 2019, ApJ, 876, 1
 Valentino, F., Magdis, G. E., Daddi, E., et al. 2020, ApJ, 890, 24
 van der Tak, F. F. S., Black, J. H., Schöier, F. L., Jansen, D. J., & van Dishoeck, E. F. 2007, A&A, 468, 627
 van Dokkum, P. G., Nelson, E. J., Franx, M., et al. 2015, ApJ, 813, 23
 Vieira, J. D., Marrone, D. P., Chapman, S. C., et al. 2013, Nature, 495, 344
 Weiß, A., Downes, D., Henkel, C., & Walter, F. 2005, A&A, 429, L25
 Weiß, A., Henkel, C., Downes, D., & Walter, F. 2003, A&A, 409, L41
 Yun, M. S., Arétxaga, I., Gurwell, M. A., et al. 2015, MNRAS, 454, 3485

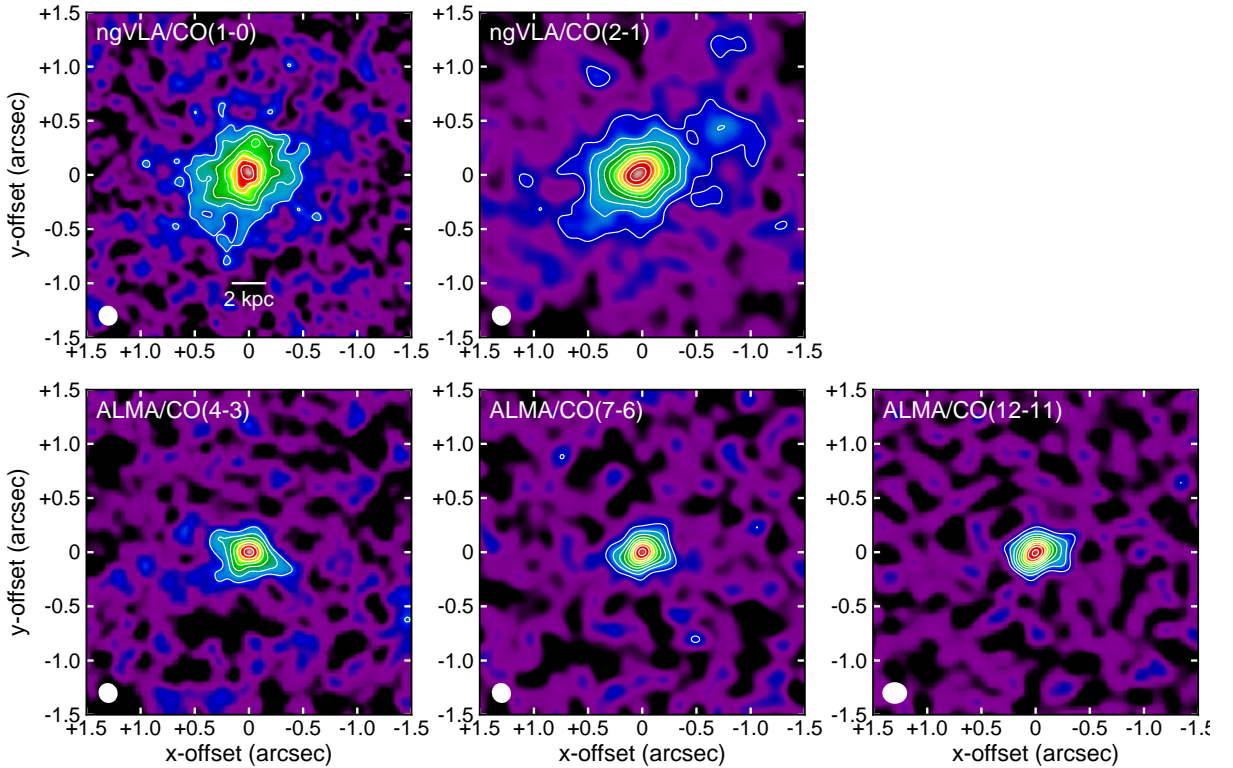


Fig. 2. The $0.^{\prime\prime}2$ (1.3 kpc)-resolution velocity-integrated flux maps of CO(1–0), CO(2–1), CO(4–3), CO(7–6), and CO(12–11) line emission are displayed. The CO(1–0) and CO(2–1) maps are created by simulations with CASA/`simobserve` task while the CO(4–3), CO(7–6) and CO(12–11) maps are real data from ALMA observations of COSMOS-AzTEC-1 at $z = 4.3$ (Tadaki et al. 2018; Tadaki et al. 2019). Contours are plotted every 2σ from 3σ .